Materials Science in Semiconductor Processing 101 (2019) 238–246

Contents lists available at ScienceDirect

Materials Science in Semiconductor Processing

journal homepage: www.elsevier.com/locate/mssp

Efficient vapor-liquid-solid synthesis of copper doped zinc oxide (Cu:ZnO) nanonails with highly homogeneous dopant distribution

Ozlem Altintas Yildirim

Konya Technical University, Faculty of Engineering and Natural Sciences, Department of Metallurgical and Materials Engineering, Konya, Turkey

ARTICLE INFO

Keywords:
Semiconducting II–VI nanostructures
Cu:ZnO nanonails
VLS growth
Homogeneous dopant distribution

ABSTRACT

Copper doped zinc oxide (Cu:ZnO) nanonails with uniformly distributed Cu ions through the nail structure were synthesized via a vapor-liquid-solid technique using seed Cu:ZnO nanoparticles. The seed nanoparticles were prepared with a simple precipitation method. The structure and morphology of nanonails and the distribution of Cu ions were investigated using X-ray diffraction, electron energy loss spectroscopy, scanning electron microscopy (SEM), transmission electron microscopy (TEM) and elemental mapping analysis. The defect states in the Cu:ZnO nanonails were characterized by room temperature photoluminescence (PL) spectra. The obtained Cu:ZnO nanonails have single phase wurtzite structure of ZnO and incorporated copper ions are in the Cu^{2+} oxidation state. SEM and TEM micrographs revealed that nanostructures with well-defined nail morphology composed of a hexagonal cap (~350 nm in diameter) and a prismatic shaft (~550 nm in diameter) connected with cylindrical neck (~250 nm in diameter). Both SEM and TEM elemental mapping analysis proved that the usage of Cu:ZnO seed nanoparticles resulted in highly homogeneous distribution of Cu ions into ZnO nanonails. High crystallinity of the Cu:ZnO nanonails was revealed with PL spectra composed of predominant second order diffraction peak and near band edge of UV emission peak and also weak defect related deep level green and violent emission peaks.

1. Introduction

With the favor of discovery of carbon nanotubes [1], one dimensional (1D) nanostructures with the specific morphology and dimension have been drawn considerable interest due to their tunable physical and chemical properties. In the last decades, 1D zinc oxide (ZnO) nanostructures provide many advantages in electrical, optoelectronic and magnetic applications due to their unique properties originating from characteristic wide band gap (3.37 eV) and large exciton binding energy (60 meV) [2].

Synthesis of 1D ZnO nanostructures with well-controlled size and shape such as nanowires [3], nanorods [4], nanocombs [5], nanobridges [6] and nanopencils [7] has been widely studied for many applications including sensor and spintronic devices [8–10]. There are three main factors exciting the researchers to work on these special morphologies; *(i)* 1D nanostructures exhibit high surface to volume ratios which provide wide opportunities for surface modification [11], *(ii)* the mismatches in the lattice constants and thermal conductivities between 1D nanostructures and substrate material are much less than that of the thin film growth on substrates [12] and *(iii)* structural and chemical characteristics can be effectively controlled during the synthesis procedure [13].

Up to now, much research have been performed to synthesize special 1D ZnO nanostructures via solution processes [14], physical vapor deposition [15], chemical vapor deposition [16], thermal evaporation [17], and vapor-liquid-solid (VLS) methods [18] etc. The VLS technique is commonly used for growing 1D nanostructures and based on the formation of liquid phase eutectic alloys with Zn vapor and catalyst particles and then condensation of 1D ZnO nanostructures on the substrate materials once reaching the supersaturation level [18,19].

Recently, ZnO nanostructures with the nanonail morphology have an increasing interest due to their unique physical, chemical and optical properties originating from their special geometries [20,21]. For example, ZnO nanonails have better filed-emission properties than that of the nanopencils due to their larger caps providing a bigger turn-on field than the nanopencils [22]. Furthermore, low-dimensional uniform ZnO nanostructures offering morphology dependent tunable magnetic properties are of particular technological interest for the spintronic applications. Although, Cu doped ZnO (Cu:ZnO) nanoneedles displayed magnetic anisotropy, Cu:ZnO nanonails exhibited the room temperature ferromagnetic properties [21,23]. Synthesis of 1D ZnO nanonails with high crystallinity can considerably improve their intrinsic properties for the usage in the various application fields such as; gas sensors, photocatalytic and photovoltaic applications.

E-mail addresses: ozlemaltintas@gmail.com, oayildirim@ktun.edu.tr.

https://doi.org/10.1016/j.mssp.2019.06.014
Received 18 March 2019; Received in revised form 10 May 2019; Accepted 11 June 2019
Available online 18 June 2019
1369-8001/

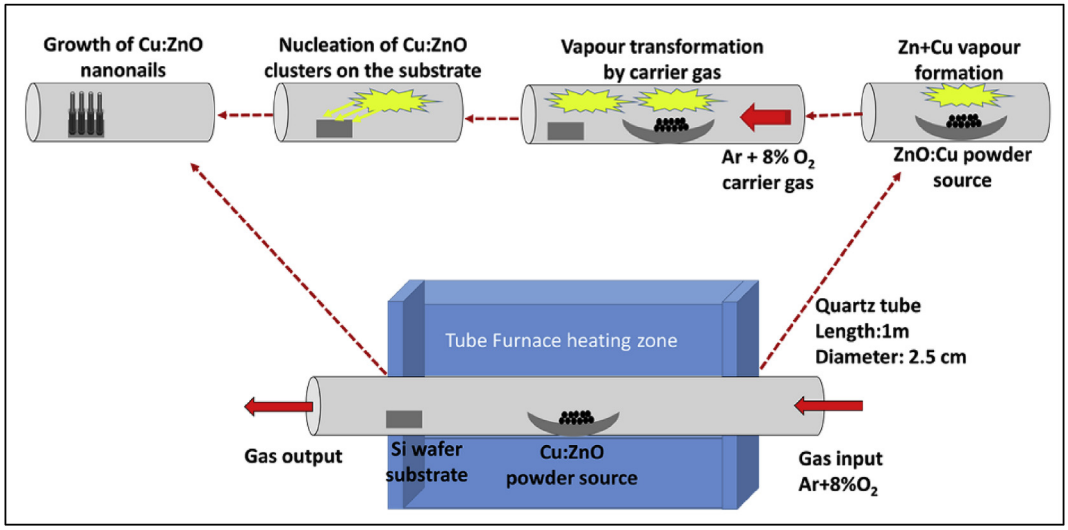

Fig. 1. The schematic illustration of setup used for the VLS growth of the Cu:ZnO nanonails from the seed Cu:ZnO nanoparticles.

Doping ZnO with suitable elements can also considerably enhance its optical, electrical and magnetic properties. Few studies have been reported on the synthesis of S, P, and Sn doped ZnO nanonails for possible applications in electronic, optoelectronic and spintronic devices [24–26]. During the last few years, Cu as a doping agent is widely employed due to the room temperature ferromagnetic behavior of Cu:ZnO nanostructures [27]. More interestingly, Cu doping can also adjust the photoluminescent transitions in ZnO by means of creating localized impurity levels [28]. Moreover, incorporation of Cu ions into the crystal structure can form new energy levels locating at 0.17 eV which is below the bottom of the conduction band of ZnO leading to an increased lifetime of the charge carriers.

For all these application fields, homogeneous distribution of Cu ions throughout the ZnO nanostructures is important to eliminate the formation of Cu-based impurities [29]. Therefore, our study aimed homogeneous distribution of Cu ions throughout the ZnO nanonails. Previous efforts to synthesize doped ZnO nanonails via VLS method were on the usage of metallic Zn and dopant ions or their oxide forms. In comparison with previous reports which suggest separate Zn and Cu powder sources for sample preparation, the usage of pre-doped seed Cu:ZnO nanoparticles provides to synthesize Cu:ZnO nanonails in which Cu ions are homogeneously distributed into ZnO structure.

In this study, we intend to explore the synthesis of Cu:ZnO nanonails by using seed nanoparticles to extent homogeneous Cu distribution throughout the ZnO crystal. For this purpose, a modified experimental conditions for the synthesis of novel hierarchical single and double-sided ZnO nanocombs was applied [5]. In here, synthesis method includes two steps; *(i)* synthesis of seed Cu:ZnO nanoparticles with ~10 nm particle size via a simple room temperature precipitation technique [27] and *(ii)* growth of nanonails via a VLS deposition technique, using the Cu:ZnO material system as seed nanoparticles.

2. Experimental procedure

The synthesis of Cu:ZnO seed nanoparticles were achieved using zinc acetate dihydrate ($C_4H_6O_4Zn{\cdot}2H_2O$, 99.5%, Fluka, Sigma-Aldrich Chemie GmbH, Steinheim, Germany), copper (II) acetate monohydrate ($(CH_3COO)_2Cu{\cdot}H_2O$, 99%, Merck KGaA, Darmstadt, Germany), polyvinylpyrrolidone ($(C_6H_9NO)_n$, PVP, MW~55000, Aldrich, Sigma-Aldrich Chemie GmbH, Steinheim, Germany) and sodium hydroxide (NaOH pellets, 97%, Merck KGaA, Darmstadt, Germany). Ethylene glycol ($C_2H_6O_2$, EG, 99%, Merck KGaA, Darmstadt, Germany) and ultra-pure deionized (DI) water were used as solvents. For growth of Cu:ZnO nanonails, graphene nanoplatelets was used to decrease the vaporization temperature of seed nanoparticles. All reagents were used without further purification.

2.1. Synthesis of seed Cu:ZnO nanoparticles

For the synthesis of seed Cu:ZnO nanoparticles, first a 0.1 M zinc-containing solution in EG was prepared. This solution was added dropwise into PVP solution (0.25 g PVP in 50 mL EG) at a rate of 50 mL/h. Then, 2 M $NaOH_{aq}$ was added into this mixture until the pH was reached to 12.7. At the same time, a separate 50 mL of aqueous copper acetate solution (2 at.% Cu:Zn ratio) was prepared. After homogenization of the solutions, copper-containing solution was slowly added into zinc-containing parent solution at a rate of 20 mL/h. Once injection completed, the final solution was homogenized for 15 min at 900 rpm. The powder products were collected by centrifugation and subsequently washed thoroughly with DI-water. The powders were then dried at 70 °C for 3 h in a vacuum dryer. To investigate the effect of Cu on the crystal structure of seed nanoparticles, same procedure was repeated without Cu addition.

2.2. Synthesis of Cu:ZnO nanonails

After synthesis of seed Cu:ZnO nanoparticles, these particles were grounded with graphene nanoplatelets to provide decomposition of precursor at lower temperatures. Then, this powder mixture was put into center of the tube furnace chamber and growth of Cu:ZnO nanostructures was let under a gas mixture of argon (98 vol %) and oxygen with 120 standard cubic centimeter per minute gas flow rate as illustrated in Fig. 1. P-type boron-doped prime Si wafers coated with 5 nm Cr (0.036 nm/s) and 10 nm Au (0.167 nm/s) thin films by electron beam deposition were used as substrates. The cleaning of the wafer surface was performed with an ultrasonicater in order of 2-proponal, acetone and then DI-water. The 2 × 2 cm silicon wafers were put into the furnace in a downstream position to collect the growth products. The tube furnace was heated to 850 °C within 1 h and kept at the same temperature for 2 h. At the end of the heating process, the furnace was cooled to room temperature over a 3 h period and a white deposit layer was observed on the surface of the wafers.

2.3. Materials characterization

The phase identification was conducted using a Bruker D2 Phaser X-ray diffractometer (XRD) in the scan range of 28–92° with a scanning rate of 0.5°/min using Cu Kα radiation (λ = 1.54 Å) and an x-ray source

operating voltage of 40 kV. The size and morphology of the seed Cu:ZnO nanoparticles and nanonails were investigated using a JEOL 7500 model scanning electron microscope (SEM) and JEOL 2100 F model transmission electron microscope (TEM). The SEM samples were examined without any conductive coating layer. The representative TEM samples were prepared simply by drying out ultrasonically dispersed aqueous suspension on holey carbon coated copper grids. Electron energy loss spectroscopy (EELS) analysis were acquired by using TEM, operated at an accelerating voltage of 200 kV. To calculate the average size of the seed nanoparticles, individual particles within the TEM images were determined by hand using commercial software (Adobe Photoshop CC) and the dimensions of the traced areas were designated using Image J, a freeware image-processing program fitting the precipitate cross-sectional areas to a best-fit sphere. The local distribution of Cu in the ZnO nanonails was employed by Energy-filtering TEM (EFTEM) mapping analyses using a Gatan environmental transfer holder to protect sample from moisture and air before loading the grid into EFTEM. The room temperature photoluminescence (PL) spectrum measurements were carried out with an excitation wavelength of 325 nm using the PerkinElmer LS 55 spectrophotometer. Any optical filter for cutting the excitation beam was not used during the measurements. DI-water was used for baseline correction for PL analyses.

3. RESULTS and DISCUSSION

3.1. Crystal structure analyses

XRD analyses were performed to assess the overall structural properties of the seed nanoparticles and VLS growth products. Fig. 2(a) represents XRD patterns of the seed 2 at.% Cu doped Cu:ZnO nanoparticles synthesized with simple precipitation method [27]. X-ray spectrum of undoped ZnO nanoparticles prepared with the same method is also given in the figure to investigate effect of Cu addition on the unit structure. For undoped ZnO nanoparticles, it was found that all peak positions of XRD diffraction lines match with a hexagonal wurtzite type crystal structure of ZnO (JCPDS card no: 36–1451). XRD pattern of the seed Cu:ZnO nanoparticles also contains same ZnO diffraction lines which indicates no trace for presence of any additional phase of copper, copper oxide(s) or any binary Zn–Cu phases within the intrinsic detection limit of XRD for phase analyses. In this study, the dopant amount of Cu was chosen below the solubility limit of Cu in ZnO [27].

Fig. 2(a) also exhibits the XRD spectrum for Cu:ZnO nanonails growth on the Au-coated Si substrate by VLS technique. The XRD pattern of the growth products also coincide with wurtzite type of ZnO structure. There is no additional peak appearance related with copper phase, but two distinctions were observed between XRD patterns of seed nanoparticles and growth products. The first one is the Si wafers originated extra peak come out at $2\theta = 69.09^\circ$ matching with (400) plane of Si. The other one is abnormal relative peak intensity observed at $2\theta = 34.36^\circ$ which corresponds to (0002) lattice plane of wurtzite ZnO structure. This singularity is attributed to the anisotropic growth of ZnO nanostructures on this crystallographic direction during the growth of the nanostructures [2].

With the heating of substrate surface, catalyst Au nanoparticles start to melt and form liquid Au droplets on the substrate surface. Zn and O vapors transferred by carrying gas hold on the Au droplets. Once, the first ZnO clusters is formed on the Si substrate, chemically active Zn-terminated polar surface provides suitable condition for local enrichment of Zn on the ZnO clusters. Therefore, (0002) surface of the cluster distributed on the substrate surface acts as a self-catalyst for the growth product. The self-catalysis effect of the polar Zn-terminated (0001) surface can explain this [0002] preferential growth orientation due to the different chemical activity of the (0001)-Zn and (0001)-O terminated polar surfaces exhibiting different growth behaviors [30]. As a result of the lowest surface energy value of the (0002) plane, ZnO grains have a tendency to grow on this direction. This explains the texture effect on XRD data with dominant (0002) reflection.

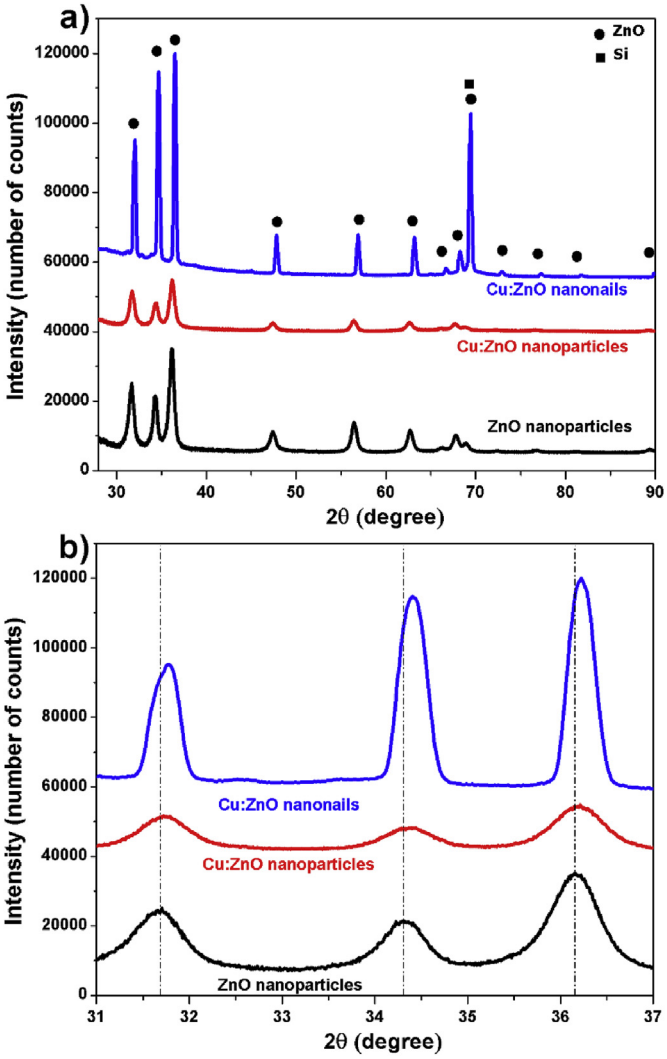

Fig. 2. (a) Overview and (b) enlarged region of the experimental XRD patterns of undoped ZnO and Cu:ZnO nanoparticles and Cu:ZnO nanonails.

Substitutional incorporation of the Cu ions into ZnO crystal can be seen with detailed XRD analysis. To investigate the possible effect of Cu addition on the crystal structure of ZnO, the diffraction lines have thoroughly been investigated. The regional XRD data shows the diffraction lines of undoped ZnO, seed Cu:ZnO nanoparticles and Cu:ZnO growth products in the 2θ range of 31–37° in Fig. 2(b). Cu doped seed nanoparticles and growth products resulted in the peak position shifts to relatively higher 2θ values than that of the undoped ZnO nanoparticles. A change in the lattice size with Cu substitution is expected due the ionic size differences between Cu (Cu^{2+}: 0.57 Å) [31] and Zn (Zn^{2+}: 0.60 Å) ions [32]. The lattice parameters (c) decreased from 5.25 Å (for pure ZnO) to 5.22 Å and 5.23 Å for seed nanoparticles and growth products, respectively. The lattice contraction due to selective/specific substitution of Cu ions with the Zn^{2+} ions in the lattice proves featly the formation of the solid solution as also reported in literature [33,34].

Close XRD comparison on the undoped ZnO nanoparticles with seed Cu:ZnO nanoparticles also revealed that the peak intensities decrement with slight increase on the peak broadening by Cu addition. This phenomena implies that dopant ions deteriorate the coherently diffracting domain size of the ZnO nanoparticles due to formation of solid solution. For the Cu:ZnO growth product, peak intensity is about four times stronger than that of seed Cu doped nanoparticles which implies the

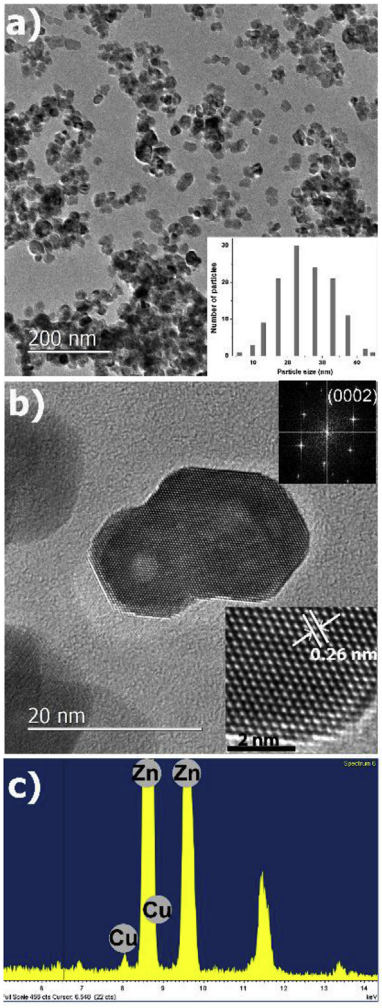

Fig. 3. (a) Low magnification TEM and (b) HR-TEM micrographs of seed Cu:ZnO nanoparticles (inset in (a) shows particle size distribution and (b) indicates corresponding SAED pattern and the closer view of particle). (c) EDX pattern of the seed nanoparticles.

high crystallinity of ZnO growth products.

3.2. Microstructural analyses

The final properties of the growth products can be affected by the physical properties of the seed nanoparticles [35]. Therefore, the size and morphology of seed Cu:ZnO nanoparticles were analyzed with TEM. Fig. 3(a) shows low magnification TEM micrograph of Cu:ZnO nanoparticles which have homogenous particle size distribution with an average particle size of 20.5 ± 1.8 nm (inset in Fig. 3(a)). Fig. 3(b) indicates atomic resolved TEM image of a selected seed Cu:ZnO nanoparticle with single crystal nature and the 0.26 nm lattice spacing corresponding to (0002) d values of hexagonal wurtzite ZnO crystal confirm the substitution of Zn^{2+} ions by Cu^{2+} ions. The corresponding selected area electron diffraction (SAED) pattern of the Cu:ZnO nanoparticles shown as an inset in the upper right of Fig. 3(b) matches with ZnO structure. As shown in the HRTEM image (lower right inset in Fig. 3(b), Cu addition forms homogeneous solid solution and does not cause any remarkable disorder or defect formation in the ZnO crystal. Compositional and quantitative analysis of seed nanoparticles were investigated using energy dispersive X-ray spectroscopy (EDS) attached with TEM (Fig. 3(c)). The EDS spectrum shows various well-defined energy lines of Zn, and lower intensity energy lines of Cu. Quantitative analysis obtained from EDS showed that the composition of the seed nanoparticles is Zn, O and Cu and the mean atomic ratio of Zn:Cu was 98.13:1.87 which is very close the initial precursor composition.

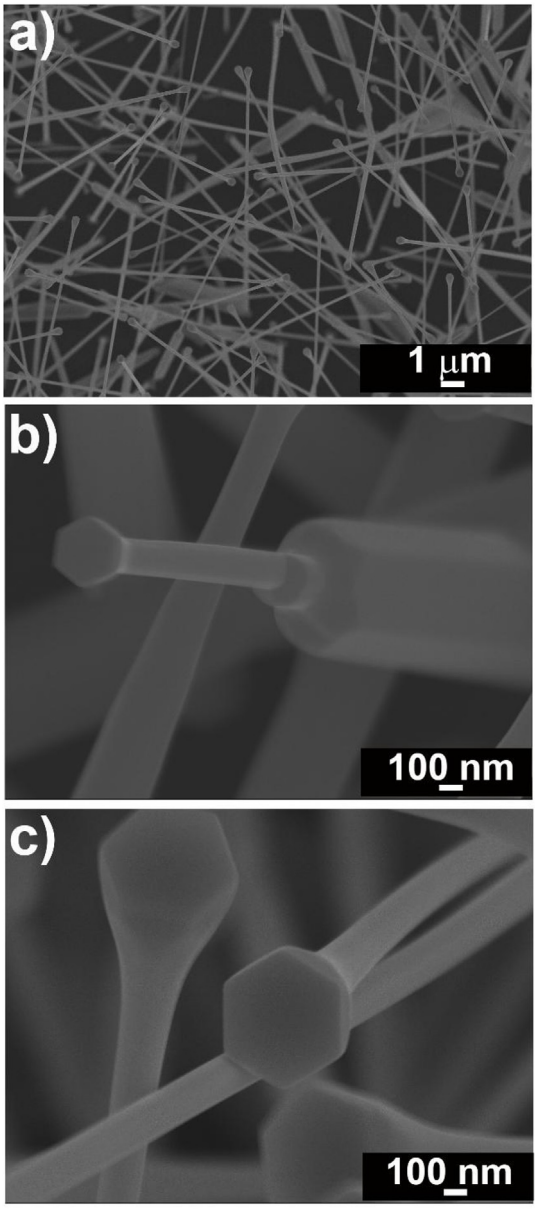

Fig. 4. (a) Low and (b–c) high magnification FESEM images of Cu:ZnO nanonails.

The growth of Cu:ZnO nanonails was carried out via a VLS technique using the Cu:ZnO seed nanoparticles to provide homogeneous distribution of Cu into ZnO growth products. FESEM analyses were used to investigate the morphology of the growth products. The FESEM micrographs revealed that the growth products as nail-shaped morphology as shown in Fig. 4(a). Fig. 4(b) exhibits a high magnification FESEM image of a selected nanonail. Typical nanonail structure is consisted of a cap and a shaft with larger diameter connected a neck having smaller diameter. The lengths are ~2.5 μm for shaft and ~6 μm for neck. It clearly shows the diameter change from the shaft to neck during the growth of the nail. Shaft has prismatic morphology with ~550 nm diameter and neck has cylindrical morphology with ~250 nm diameter. Fig. 4(c) exhibits close view image of the nail caps. They have well defined hexagonal shape with ~350 nm cap diameter and ~190 nm hexagonal edge length.

Studies related with the synthesis of doped ZnO nanonails have mainly focused on the optical and magnetic properties of these doped

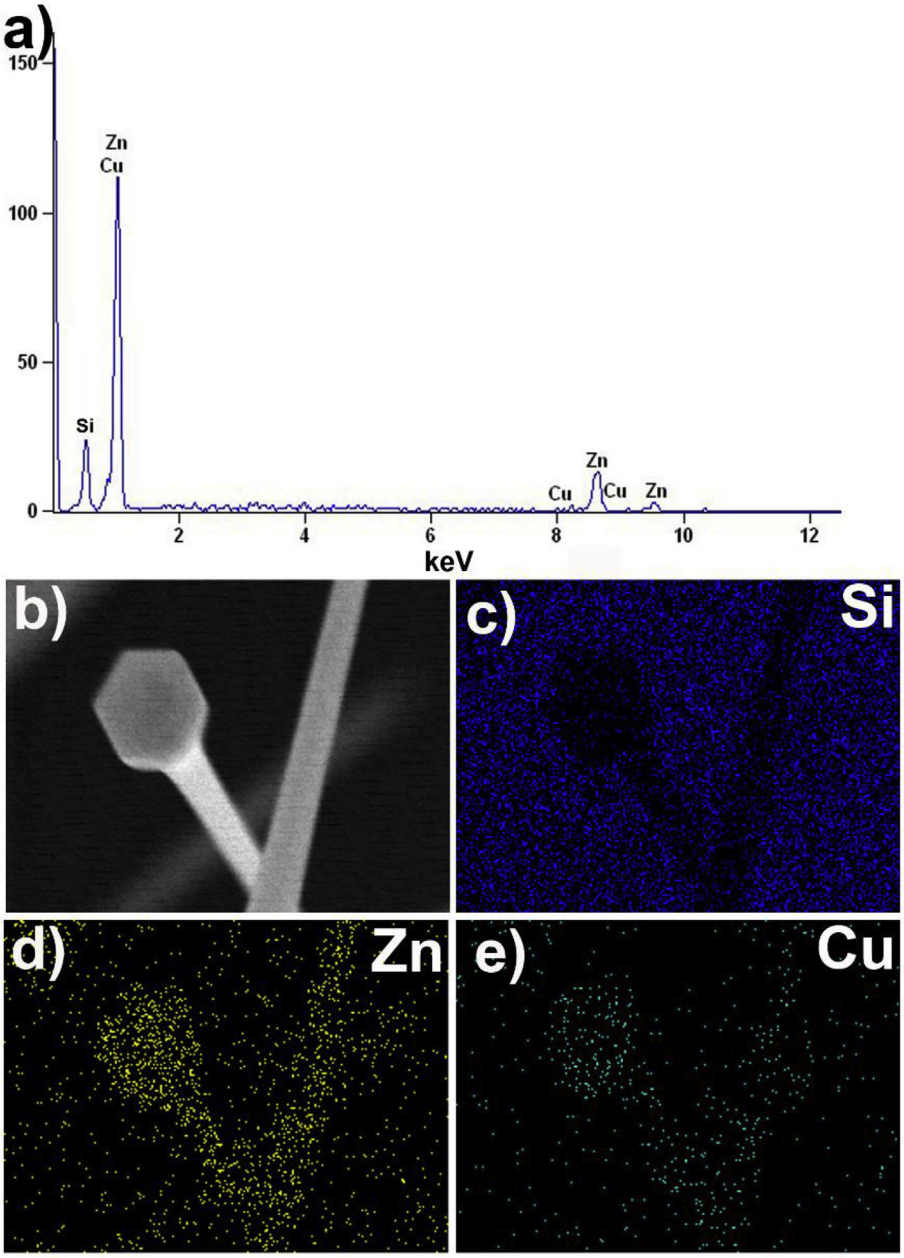

Fig. 5. (a) EDX spectrum, (b) SEM image and (c–e) elemental EDX mapping images of the Si, Zn and Cu of Cu:ZnO nanonails.

structures [21,24,26]. However, homogeneous distribution of dopant ions has been taken less attention. The composition of the cap and neck parts in the Cu:ZnO nanonails were investigated using EDS attached with FESEM as shown in Fig. 5(a). EDS measurement of the Cu:ZnO nanonails showed various well defined energy lines of Zn, Cu and Si. The Si signal was attributed to wafer substrate. The atomic content of Cu was determined as 1.63 at.%. The rest of the Cu content is exhausted with the carrier gas flow. To investigate Cu distribution, elemental mapping analysis of ZnO nanonails was performed. The typical FESEM micrograph taken for the elemental mapping shows the cap and neck region of the selected nanonails in Fig. 5(b). Fig. 5(c–e) exhibit elemental mapping images of Si, Zn and Cu. The dense spot of Si signal comes from outside of the nanonails which is evidence of Si arising from the substrate. EDS elemental map images of Zn and Cu prove that Cu atoms were homogeneously distributed throughout the ZnO crystal.

The homogeneous distribution of the dopant ions into ZnO crystal is important at the atomic level for the conclusive properties of the ZnO nanostructures. Fig. 6 represents TEM micrographs of Cu:ZnO nanonails. Low magnification TEM image (Fig. 6(a)) indicates the smooth surface of Cu:ZnO nanonail and any trace for amorphous layer is not detected throughout the surface. HR-TEM micrographs taken from the marked area of the neck and cap regions in the low magnification TEM image are shown in Fig. 6(b and c), respectively. No observable defects or second phase precipitation strongly advise that Cu atoms are well-incorporated into the ZnO lattice. Fringes of individual atomic planes are clearly visible in the micrograph and indicate the single crystalline nature of the Cu:ZnO nanonails preserving the growth direction along the c-axis. The measured interplanar spacing is about 0.26 nm, corresponding to the (0002) plane of ZnO. The representative SAED pattern taken from the HRTEM image shows that the growth direction is [0001] (inset in Fig. 6(b and c)) which is agreed with the XRD results (Fig. 2). Thus, we can conclude that the lattice structure of ZnO crystal are not drastically distorted with Cu doping.

In order to examine accurate atomic scale distribution of Cu in the ZnO lattice, EFTEM analyses were performed. Fig. 7(a and b) show elemental mapping images of Zn and Cu obtained by EFTEM. The dense

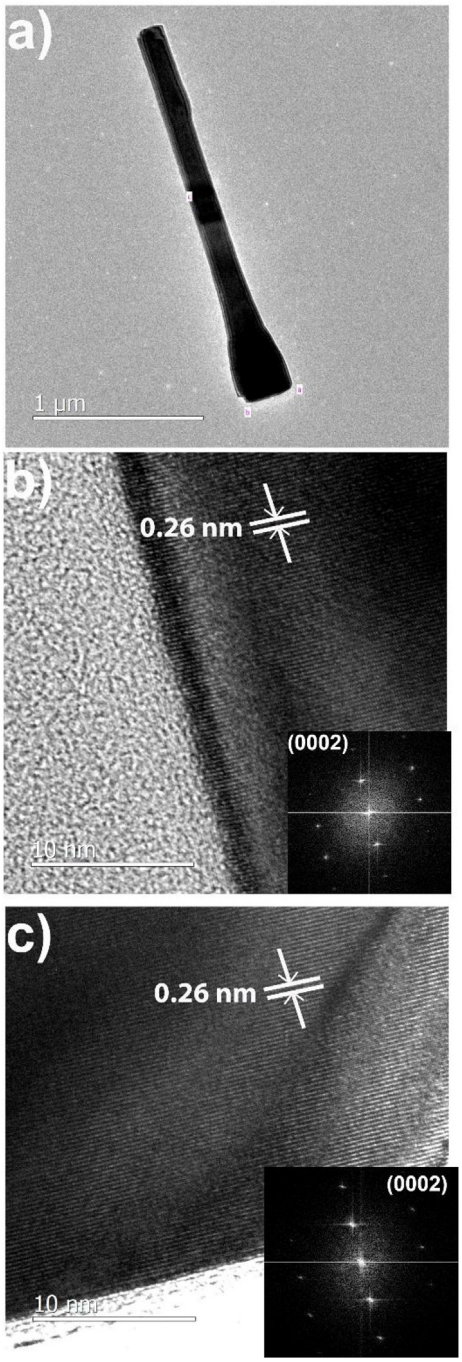

Fig. 6. (a) Low magnification TEM and (b–c) HR-TEM micrographs of Cu:ZnO nanonails (insets show corresponding SAED patterns).

brighter points representing higher concentration of the elements confirm that the nanonail is ZnO. EFTEM analysis also reveals that Cu doping occurs homogeneously throughout the nail structure at atomic scale.

EELS analysis which is an effective technique for material characterization with a nanometer resolution was employed in the exploration of the oxidation state of the Cu ions in the wurtzite structure. In the EELS, the transition-metal elements usually exhibit sharp L ionization edge peaks at the near edge region which are known as white lines. The transition of an electrons from $2p_{3/2}$ level to $3d_{3/2}$ state and $2p_{1/2}$ level to $3d_{3/2}$ state result in the formation of L3 and L2 white lines [36]. Cu white lines are observed at $\Delta E = 930$ eV (Cu L3) and $\Delta E = 950$ eV (Cu L2) [37,38]. L3 and L2 white lines are separated by about 20 eV due to the spin orbit splitting of the 2p core hole. The relative intensity ratio of L3 and L2 white lines gives information about the unoccupied states in the 3d bands. Thus, the oxidation state of the Cu in the nanonails can be determined by EELS [39]. Fig. 7(c) exhibits EELS spectra of Cu:ZnO nanonails. In the spectrum, the energy loss of the L shell edge of Zn ($\Delta E = 1020$ eV) and L3 white line of Cu ($\Delta E = 930$ eV) marked with red dashed cycle are clearly observed. Less distinct L2 white line of Cu is also present in the spectra. L3-L2 ratio is usually much greater than 2:1, thus; lower intensity of L2 line is the expected result [40]. As already known, metallic state Cu with the full 3d states indicates no white lines. Therefore, the presence of sharp L3 and less distinct L2 white lines indicate the electron transitions between the energy levels and a depletion of the electron/atom from 3d states. The locations and shapes of L2 and L3 EELS edges of Cu give access to the information about the ionic state of Cu. Unlike the metallic Cu with no white lines, monovalent Cu (Cu^{1+}) generates strong and asymmetric L3 and L2 peaks. Meanwhile, for divalent Cu ion (Cu^{2+}), the Cu L3 and L2 edges characteristically exhibits symmetric peaks [41]. Therefore, symmetric shape L3 peak in the spectra indicates that Cu presents in the wurtzite nanonails in the Cu^{2+} oxidation state.

3.3. Optical analyses

The room temperature PL spectra was recorded to explore the defect generation and optical properties of ZnO nanonails (Fig. 8). The spectrum for nanonails can be divided into four different emission bands. Deconvolution of the overlapping peaks were performed by Gaussian fitting using Origin 2018 software. The first distinct one belongs to the second order band edge emission at ~1.67 eV (740 nm) which appears in only nanostructured material systems with peculiar UV emission peak and indicates higher crystalline structure [42,43]. This result has good agreement with the XRD data. The broad emission peaks appeared at 2.42 eV and 3.03 eV are related with defects. The former emission peak (2.42 eV) can be attributed to the deep level green emission originated by the electron transfer from conduction band to the oxygen vacancy level [44]. The latter peak (3.03 eV) can be assigned to violet emission originated by the electron transfer from conduction band to the zinc vacancy level [45]. According to spectra, the relative peak intensity of green emission is lower than that of the violet emission. This can be explained with two phenomena. (i) During the growth of nanonails, the continuous supply of oxygen by the carrying gas boost resulted in the low generation of the oxygen vacancy site. (ii) At the end of evaporation of seed nanoparticles, the exhaustion of Zn vapor providing the cap formation on the neck of the nanonails resulted in the high generation of the zinc vacancy site. The last peak appeared at 3.26 eV is the strongest emission peak among the four peaks. This near band edge UV emission peak is responsible for the recombination of free excitons through an exciton - exciton collusion process and corresponding to band gap of bulk ZnO [2,46].

3.4. Growth mechanism of nanonails structure

The FESEM and TEM analysis show that VLS growth Cu:ZnO products have very similar nail-like morphologies. During the growth process, achievement of the sufficient temperature results in the formation of liquid Au droplets by reducing the surface energy of catalyst thin Au film on the surface of substrates. These liquid Au droplets provide a proper environment for the growth of the nail structures.

In the previous report, single-sided ZnO nanocomb structure was synthesized via similar VLS method in a different growth temperature [5]. Relatively higher growth temperature, 1000 °C, in the synthesis of comb structure, molten Au film forms broad liquid Au islands enabling to grow flower structure having many branches. However, in the synthesis of nanonails, lower growth temperature, 850 °C, provides creation of small-sized Au spheres instead of the formation of large Au islands. These small Au spheres lead to hold Zn and O vapors for the

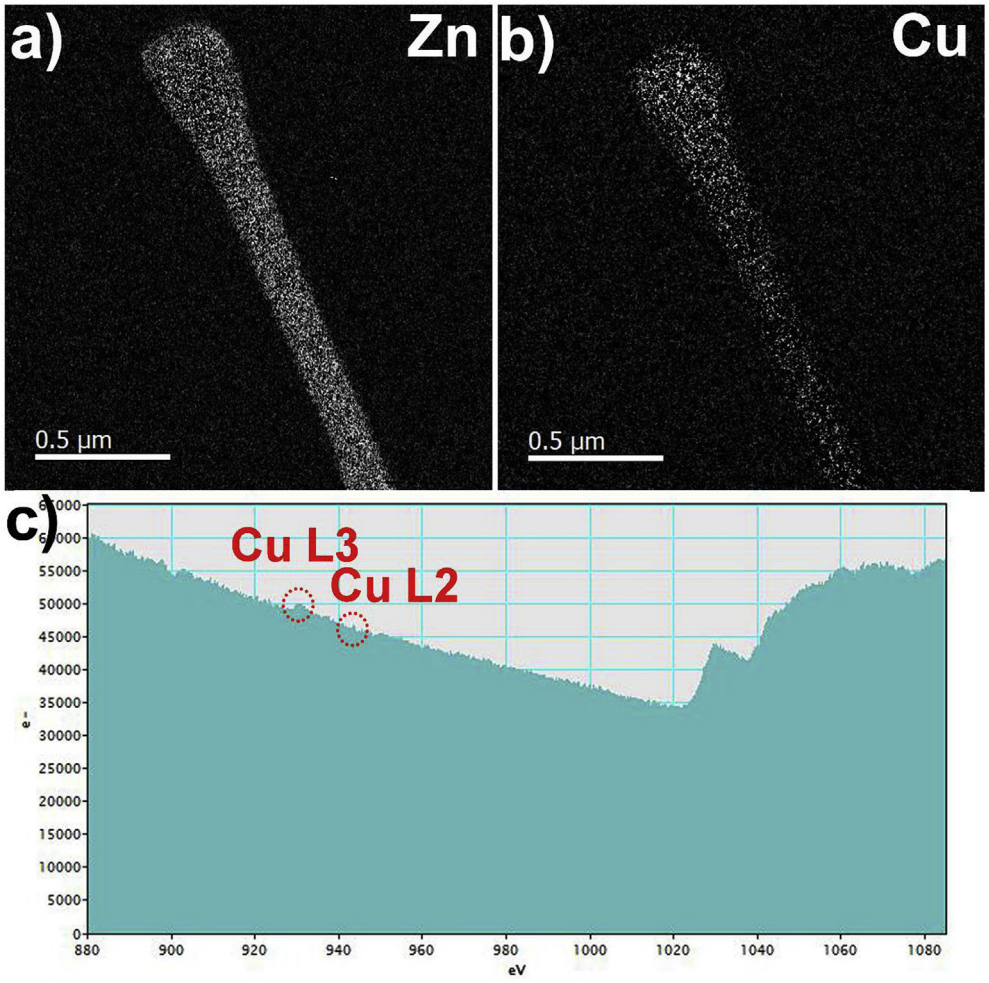

Fig. 7. (a) Zn and (b) Cu elemental mapping images obtained by EFTEM and (c) EELS spectra of Cu:ZnO nanonails.

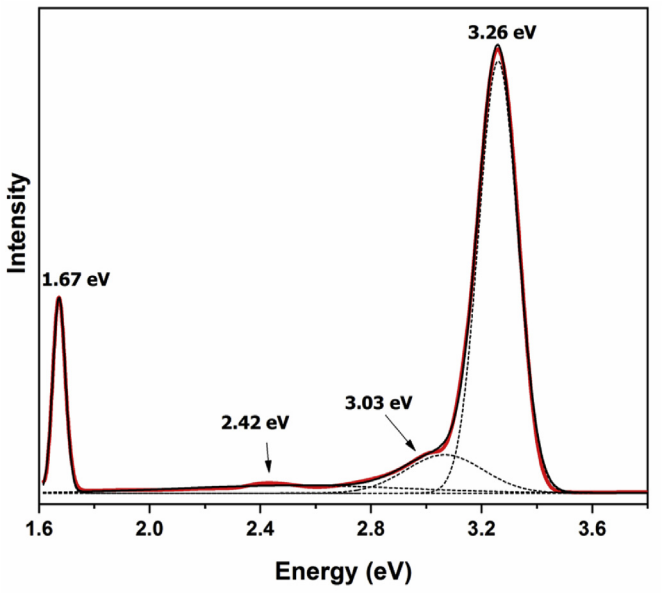

Fig. 8. PL spectra of Cu:ZnO nanonails.

formation of ZnO clusters. This temperature related tunable morphology is similar to the observation reported by Shen et al. [7,47]. They found that different dimension and morphology from the nanopencils to nanonails can be fabricated by tuning the evaporation temperature of catalyst indium powders.

During the synthesis, vapor of the source powders was obtained with heating of the seed nanoparticles and moved to the low temperature region by the carrier-gas mixture. The moved vapor containing Zn and Cu formed first Cu:ZnO nucleates on the small Au sphere regions of Si substrates. Further evaporation of the seed nanoparticles caused to germinate Cu:ZnO nanorods. As a result of continuous deposition and growth of Cu:ZnO nanorods in the [0002] preferential growth direction, prismatic shaft parts of the nanonails formed. With the continuous growth of the Cu:ZnO shaft, the amount of the seed powder vaporization diminished; thus, few Cu:ZnO vapor deposited on the upper part of the shaft and formed the smaller diameter neck than that of the shaft.

The formation of hexagonal cap comes up ultimate of the growth process. The research conducted by Yan et al. [48] indicates that the formation of the nanonail-shaped ZnO structure can be explained with the changes in the supersaturation rate of ZnO vapor by the formation and split of a thin shell layer on the powder source. At relatively low temperature, supersaturation rate is high which induces 1D growth, however, at moderate temperature, a thin ZnO shell layer is formed on the powder source as a result of dropping and collapsing vaporized ZnO with a decrement on the supersaturation rate relative to the initial stage. Along with the heating, the ZnO vapor pressure would increase under the shell due to the continuous evaporation of ZnO source and once critical pressure is reached, shell layer would be split and supersaturation rate suddenly increases. Maximum lateral growth rate is shown in 2D growth in conjunction with formation of the symmetrical

hexagonal nanoplate cap as a result of increment of supersaturation rate. Due to shadow effect, the upper part of the nail is more exposed to carrying gas mixture which transfer simultaneously Zn and Cu vapors and thus to more ion bombardment resulted faster axial growth rate than that of the neck part. Therefore, upper part of the nail grows bigger and forms cap structure.

4. Conclusions

In summary, Cu:ZnO nanonails consisted of a hexagonal shaped cap with ~350 nm cap diameter and a shaft with ~550 nm in diameter and ~2.5 μm in length connected a neck with ~250 nm in diameter and ~6 μm in length were grown via VLS method. Uniformly distributed Cu ions from shaft to cap of nanonails proved by the elemental mapping and EFTEM analysis was achieved using seed Cu:ZnO nanoparticles seed nanoparticles as a source material. The detailed structural analysis information performed by XRD displayed that Cu addition did not change the wurtzite structure but a shift of the diffraction peak position was observed due to substitutionally incorporation of Cu ions into ZnO structure. Ionic state of copper was determined as Cu^{2+} by EELS analysis. The PL spectra of nanonails are composed of strong second order diffraction and near band edge UV emission peaks which indicate high crystallite structure of nanonails. Weak violent emission related with zinc vacancy defect levels originated from the exhaustion of Zn vapor at the end of the nanonails growth providing the formation of the cap on the neck part of the nail. Such a homogeneous doping model can open the door for designing new class homogeneously doped semiconductor nanostructures with other dopant elements for various potential applications.

Acknowledgments

The author is grateful to Amanda K. Petford-Long and Yuzi Liu for providing access to Center for Nanoscale Materials, Argonne National Laboratory, USA and also thanks them for their invaluable assistance in the analyses and helpful comments. The author wishes to thank Ilyas Savkliyildiz for his fruitful discussions. OAY thanks for support by the Scientific Research Foundation of Selcuk University under Project No. 15401123 for the financial support of this research.

Appendix A. Supplementary data

Supplementary data to this article can be found online at https://doi.org/10.1016/j.mssp.2019.06.014.

References

[1] S. Iijima, Helical microtubules of graphitic carbon, Nature 354 (1991) 56.
[2] T. Van Khai, L. Van Thu, L.T.T. Ha, V.M. Thanh, T.D. Lam, Structural, optical and gas sensing properties of vertically well-aligned ZnO nanowires grown on graphene/Si substrate by thermal evaporation method, Mater. Char. 141 (2018) 296–317.
[3] P.X. Gao, Z.L. Wang, Substrate atomic-termination-induced anisotropic growth of ZnO nanowires/nanorods by the VLS process, J. Phys. Chem. B 108 (23) (2004) 7534–7537.
[4] A. Saboor, S.M. Shah, H. Hussain, Band gap tuning and applications of ZnO nanorods in hybrid solar cell: Ag-doped verses Nd-doped ZnO nanorods, Mater. Sci. Semicond. Process. 93 (2019) 215–225.
[5] O. Altintas Yildirim, Y. Liu, A.K. Petford-Long, Synthesis of uniformly distributed single- and double-sided zinc oxide (ZnO) nanocombs, J. Cryst. Growth 430 (2015) 34–40.
[6] J. Lao, J. Huang, D. Wang, Z. Ren, ZnO nanobridges and nanonails, Nano Lett. 3 (2) (2003) 235–238.
[7] G. Shen, Y. Bando, B. Liu, D. Golberg, C.J. Lee, Characterization and field-emission properties of vertically aligned ZnO nanonails and nanopencils fabricated by a modified thermal-evaporation process, Adv. Funct. Mater. 16 (3) (2006) 410–416.
[8] R. Saravanan, K. Santhi, N. Sivakumar, V. Narayanan, A. Stephen, Synthesis and characterization of ZnO and Ni doped ZnO nanorods by thermal decomposition method for spintronics application, Mater. Char. 67 (2012) 10–16.
[9] Y. Wei, X. Wang, G. Yi, L. Zhou, J. Cao, G. Sun, Z. Chen, H. Bala, Z. Zhang, Hydrothermal synthesis of Ag modified ZnO nanorods and their enhanced ethanol-sensing properties, Mater. Sci. Semicond. Process. 75 (2018) 327–333.
[10] S. Goutham, S. Kaur, K.K. Sadasivuni, J.K. Bal, N. Jayarambabu, D.S. Kumar, K.V. Rao, Nanostructured ZnO gas sensors obtained by green method and combustion technique, Mater. Sci. Semicond. Process. 57 (2017) 110–115.
[11] H.W. Ra, R. Khan, J.T. Kim, B.R. Kang, K.H. Bai, Y.H. Im, Effects of surface modification of the individual ZnO nanowire with oxygen plasma treatment, Mater. Lett. 63 (28) (2009) 2516–2519.
[12] R. Ghosh, D. Basak, S. Fujihara, Effect of substrate-induced strain on the structural, electrical, and optical properties of polycrystalline ZnO thin films, J. Appl. Phys. 96 (5) (2004) 2689–2692.
[13] P. Yang, H. Yan, S. Mao, R. Russo, J. Johnson, R. Saykally, N. Morris, J. Pham, R. He, H.J. Choi, Controlled growth of ZnO nanowires and their optical properties, Adv. Funct. Mater. 12 (5) (2002) 323–331.
[14] L.E. Greene, M. Law, J. Goldberger, F. Kim, J.C. Johnson, Y. Zhang, R.J. Saykally, P. Yang, Low-temperature wafer-scale production of ZnO nanowire arrays, Angew. Chem. 115 (26) (2003) 3139–3142.
[15] Y. Kong, D. Yu, B. Zhang, W. Fang, S. Feng, Ultraviolet-emitting ZnO nanowires synthesized by a physical vapor deposition approach, Appl. Phys. Lett. 78 (4) (2001) 407–409.
[16] A. Sáenz-Trevizo, P. Amézaga-Madrid, P. Pizá-Ruiz, W. Antúnez-Flores, C. Ornelas-Gutiérrez, M. Miki-Yoshida, Single and multi-layered core-shell structures based on ZnO nanorods obtained by aerosol assisted chemical vapor deposition, Mater. Char. 105 (2015) 64–70.
[17] S.Y. Bae, C.W. Na, J.H. Kang, J. Park, Comparative structure and optical properties of Ga-, In-, and Sn-doped ZnO nanowires synthesized via thermal evaporation, J. Phys. Chem. B 109 (7) (2005) 2526–2531.
[18] M.H. Huang, Y. Wu, H. Feick, N. Tran, E. Weber, P. Yang, Catalytic growth of zinc oxide nanowires by vapor transport, Adv. Mater. 13 (2) (2001) 113–116.
[19] P.X. Gao, Z.L. Wang, Substrate atomic-termination-induced anisotropic growth of ZnO nanowires/nanorods by the VLS process, J. Phys. Chem. B 108 (23) (2004) 7534–7537.
[20] A. Umar, M.M. Rahman, S.H. Kim, Y.-B. Hahn, Zinc oxide nanonail based chemical sensor for hydrazine detection, Chem Commun (2) (2008) 166–168.
[21] Z. Zhang, J.B. Yi, J. Ding, L.M. Wong, H.L. Seng, S.J. Wang, J.G. Tao, G.P. Li, G.Z. Xing, T.C. Sum, Cu-doped ZnO nanoneedles and nanonails: morphological evolution and physical properties, J. Phys. Chem. C 112 (26) (2008) 9579–9585.
[22] G.Z. Shen, Y. Bando, B.D. Liu, D. Golberg, C.J. Lee, Characterization and field-emission properties of vertically aligned ZnO nanonails and nanopencils fabricated by a modified thermal-evaporation process, Adv. Funct. Mater. 16 (3) (2006) 410–416.
[23] T. Herng, S. Lau, S. Yu, H. Yang, L. Wang, M. Tanemura, J. Chen, Magnetic anisotropy in the ferromagnetic Cu-doped ZnO nanoneedles, Appl. Phys. Lett. 90 (3) (2007) 032509.
[24] G. Shen, J.H. Cho, J.K. Yoo, G.-C. Yi, C.J. Lee, Synthesis and optical properties of S-doped ZnO nanostructures: nanonails and nanowires, J. Phys. Chem. B 109 (12) (2005) 5491–5496.
[25] J.-Y. Zhang, Q.-F. Zhang, T.-S. Deng, J.-L. Wu, Electrically driven ultraviolet lasing behavior from phosphorus-doped p-ZnO nanonail array/n-Si heterojunction, Appl. Phys. Lett. 95 (21) (2009) 211107.
[26] W.E. Mahmoud, T. Al-Harbi, Synthesis, characterization and photoluminescence properties of Sn doped ZnO nanonails, J. Cryst. Growth 327 (1) (2011) 52–56.
[27] Ö. Altıntaş Yıldırım, C. Durucan, Room temperature synthesis of Cu incorporated ZnO nanoparticles with room temperature ferromagnetic activity: structural, optical and magnetic characterization, Ceram. Int. 42 (2, Part B) (2016) 3229–3238.
[28] C. Xu, X. Sun, X. Zhang, L. Ke, S. Chua, Photoluminescent properties of copper-doped zinc oxide nanowires, Nanotechnology 15 (7) (2004) 856.
[29] L.-H. Ye, A.J. Freeman, B. Delley, Half-metallic ferromagnetism in Cu-doped ZnO: density functional calculations, Phys. Rev. B 73 (3) (2006) 033203.
[30] Z.L. Wang, X.Y. Kong, J.M. Zuo, Induced growth of asymmetric nanocantilever arrays on polar surfaces, Phys. Rev. Lett. 91 (18) (2003) 185502.
[31] R. Shannon, Revised effective ionic radii and systematic studies of interatomic distances in halides and chalcogenides, Acta Crystallogr., Sect. A: Found. Crystallogr. 32 (5) (1976) 751–767.
[32] B.D. Ahn, H.S. Kang, J.H. Kim, G.H. Kim, H.W. Chang, S.Y. Lee, Synthesis and analysis of Ag-doped ZnO, J. Appl. Phys. 100 (9) (2006) 093701-093701-6.
[33] G. Shukla, Magnetic and optical properties of epitaxial n-type Cu-doped ZnO thin films deposited on sapphire substrates, Appl. Phys. A 97 (1) (2009) 115–118.
[34] Z. Zhang, J.B. Yi, J. Ding, L.M. Wong, H.L. Seng, S.J. Wang, J.G. Tao, G.P. Li, G.Z. Xing, T.C. Sum, C.H. Alfred Huan, T. Wu, Cu-doped ZnO nanoneedles and nanonails: morphological evolution and physical properties, J. Phys. Chem. C 112 (26) (2008) 9579–9585.
[35] Z.L. Wang, Splendid one-dimensional nanostructures of zinc oxide: a new nanomaterial family for nanotechnology, ACS Nano 2 (10) (2008) 1987–1992.
[36] W. Waddington, P. Rez, I. Grant, C. Humphreys, White lines in the L 2, 3 electron-energy-loss and x-ray absorption spectra of 3d transition metals, Phys. Rev. B 34 (3) (1986) 1467.
[37] S.Y. Bae, H.W. Seo, J. Park, Vertically aligned sulfur-doped ZnO nanowires synthesized via chemical vapor deposition, J. Phys. Chem. B 108 (17) (2004) 5206–5210.
[38] R. Leapman, L. Grunes, P. Fejes, Study of the L 23 edges in the 3 d transition metals and their oxides by electron-energy-loss spectroscopy with comparisons to theory, Phys. Rev. B 26 (2) (1982) 614.
[39] D. Pearson, C. Ahn, B. Fultz, Measurements of 3d occupancy from Cu L 2, 3 electron-energy-loss spectra of rapidly quenched CuZr, CuTi, CuPd, CuPt, and CuAu, Phys. Rev. B 50 (17) (1994) 12969.
[40] R. Leapman, L. Grunes, Anomalous L 3 L 2 white-line ratios in the 3 d transition

metals, Phys. Rev. Lett. 45 (5) (1980) 397.
[41] L. Laffont, M. Wu, F. Chevallier, P. Poizot, M. Morcrette, J.-M. Tarascon, High resolution EELS of Cu–V oxides: application to batteries materials, Micron 37 (5) (2006) 459–464.
[42] V. Srikant, D.R. Clarke, On the optical band gap of zinc oxide, J. Appl. Phys. 83 (10) (1998) 5447–5451.
[43] Y.G. Wang, S.P. Lau, H.W. Lee, S.F. Yu, B.K. Tay, X.H. Zhang, H.H. Hng, Photoluminescence study of ZnO films prepared by thermal oxidation of Zn metallic films in air, J. Appl. Phys. 94 (1) (2003) 354–358.
[44] C.H. Ahn, Y.Y. Kim, D.C. Kim, S.K. Mohanta, H.K. Cho, A comparative analysis of deep level emission in ZnO layers deposited by various methods, J. Appl. Phys. 105 (1) (2009) 013502.
[45] S.-H. Jeong, B.-S. Kim, B.-T. Lee, Photoluminescence dependence of ZnO films grown on Si (100) by radio-frequency magnetron sputtering on the growth ambient, Appl. Phys. Lett. 82 (16) (2003) 2625–2627.
[46] A. Kalita, M.P.C. Kalita, Effects of size reduction on microstructural, optical, vibrational, magnetic and photocatalytic properties of ZnO nanocrystals, Mater. Char. 137 (2018) 109–118.
[47] G. Shen, J.H. Cho, C.J. Lee, Morphology-controlled synthesis, growth mechanism and optical properties of ZnO nanonails, Chem. Phys. Lett. 401 (4–6) (2005) 414–419.
[48] Y.G. Yan, L.X. Zhou, Z.D. Han, Y. Zhang, Growth analysis of hierarchical ZnO nanorod array with changed diameter from the aspect of supersaturation ratio, J. Phys. Chem. C 114 (9) (2010) 3932–3936.